Thermomechanical analysis of two-dimensional boron monolayers

Thierry Tsafack and Boris I. Yakobson

Thermomechanical analysis of two-dimensional boron monolayers

Thierry Tsafack and Boris I. Yakobson

Department of Materials Science and Nanoengineering, Rice University, 6100 Main MS-325,

Houston, TX, USA 77005-1827

Abstract

Using density functional theory calculations (both perturbed and unperturbed) as well as thermodynamic and ballistic transport equations, what follows investigates thermal and mechanical properties of 2D boron monolayers (δ_6-, α-, δ_5-, and χ_3-sheets with respective vacancy densities $\eta = 0$, 1/9, 1/7, 1/5) as they relate to the vacancy density. The triangular (δ_6) sheet's room-temperature phonon and electron thermal conductances are found to respectively be roughly 2.06 times and 6.60 times greater than those of graphene. The Young's moduli, calculated from longitudinal and transverse sound velocities are in good agreement with those obtained from elastic constants. Values range from 171 to 619 N/m, two of which (619 N/m for α-sheet and 546 N/m δ_5-sheet) exceed graphene's Young's modulus (~340 N/m). It is determined that the vacancy density have a diminishing effect on both the phonon heat capacity at constant volume and the phonon ballistic thermal conductance, but no regular correlation on the electron heat capacity and electron ballistic thermal conductance.

I. Introduction

Like carbon, boron is one of the few elements with pure, freestanding, and single-layer structures. Starting from a bi-dimensional repetition of equilateral triangles, a plethora of such 2D structures have been predicted[1-5] by increasing the ratio of hexagon holes to the number of atomic sites in the original triangular sheet within one unit cell, namely, the hexagonal vacancy density η. Plus, a relationship among the vacancy density, the stability, and the morphology of boron sheets has been abduced[1-6]. Stable boron

1

sheets with η between and including 0 and 1/9 are buckled. Those with η between 1/9 and 1/5 (excluding the former and including the latter) are flat. Those with η greater than, and excluding 1/5, are unstable.

Among all the predicted boron sheets, the synthesis of δ_6 (η = 0), β_{12} (η = 1/6) and χ_3 (η = 1/5) have recently been reported[7-9], albeit weakly bounded to the substrate. The synthesis of δ_6[9] was done under ultrahigh vacuum conditions using a solid boron atomic source as a precursor and atomic scale characterization to confirm its predicted anisotropic buckling. The synthesis of β_{12}[8] and χ_3[8] were done on Ag(111) surface in ultrahigh vacuum chamber employing molecular beam epitaxy (MBE) thereby confirming their flat morphology. Earlier[10] and subsequent computational studies[9] further confirmed the anisotropic nature of elastic moduli of δ_6.

Given the relevance of the vacancy density to the stability and shape of 2D boron sheets, its impact on thermal properties is not only to be expected but also worth exploring, which is what the present investigation purports to do. The phonon and electron heat capacity at constant volume per unit area along with the phonon and electron thermal conductances are calculated on the basis of the previously calculated phonon spectra and electronic band structures for four boron sheets: δ_6-, α-, δ_5-, and χ_3- (with vacancy densities η = 0, 1/9, 1/7, and 1/5 respectively). The lattice and electronic band structures are calculated using the density functional perturbation theory (DFPT) and the density functional theory (DFT) implemented in the *Quantum Espresso* package[11], whereas thermal properties are computed using well-known thermal equations[12,13]. The lattice and electronic thermal conductances are computed implementing ballistic transport equations[14,15] for 2D materials. Longitudinal and transverse sound velocities, extracted as slopes of acoustic branches, are used to estimate the Young's modulus and Poisson's ratio of hexagonal and non-hexagonal 2D boron lattices.

The previous properties are also compared and contrasted with the same properties calculated for graphene in view of its high lattice thermal conductance. A more minute rendition of the theoretical and computational framework is laid out in the next section. The presentation of, the comments on, the discussions about, and the conclusions from the results will ensue in the successive section.

II. MODELS AND METHODS

A. Phonon and electronic spectra

Both DFT and DFPT calculations were performed using their numerical implementations in *Quantum Espresso*[11]. Initial lattice parameters, angles, atomic positions and symmetries for δ_6-, δ_5-, and χ_3-sheets are taken from Kunstmann *et al.*[10] and Wu *et al.*[6] (see **TABLE I.** for relaxed structural parameters). The geometry optimization was done setting the plane-wave cutoff energy to 500 eV, the total energy convergence criterion to 5.0 μeV/atom, the criterion for the force on all atoms to less than 2.0 meV/atom, and the vacuum distance to 30 Å. The ultra-soft pseudo-potentials and the exchange-correlation functionals in the form of Perdew-Burke-Ernzerhof (PBE) within the generalized gradient approximation (GGA)[16] are used in all calculations.

TABLE I. Relaxed structural parameters . Lattice constants (a, b), angle (γ) between $\vec{a}$ and $\vec{b}$, buckling and space groups for δ_6, α, δ_5, and χ_3.

	δ_6		α		δ_5		χ_3	
a (Å)	3.30	2.82[a]	5.10	5.046[b]	4.54	4.47[b]	2.97	2.90[b]
b (Å)	1.61	1.60[a]	5.10	5.044[b]	4.54	4.47[b]	4.54	4.44[b]
γ (º)	59.24	90.00[a]	120.00	59.99[b]	60.00	120.00[b]	70.89	70.95[b]
Buckling (Å)	0.89	0.82[a]	0.14	0.17[b]	0.00	0.00[b]	0.00	0.00[b]
Space group	p1	pm[a]	p3	p3[b]	p3	p3[b]	p1	p1[b]

[a] Kunstmann *et al.*[10]

[b] Wu *et al.*[6]

Wu *et al.*[6] used first-principles particle swarm optimization (PSO) to stabilize the originally unstable α-sheet resulting into a structure with every two adjacent atoms (with coordination number 6) moving upward and downward outside of the plane by the same amount, 0.17 Å. In the said study, the lattice constants are slightly different, 5.046 Å vs 5.044 Å. The approach used in this investigation entailed: 1) relaxing randomly and slightly buckled α-sheets, and 2) selecting the structure with the minimum energy.

Unlike α'-sheet proposed by Wu *et al.*[6], the previous approach resulted in a structure similar to the original α-sheet with the lattice constants being equal (5.10 Å), and adjacent boron atoms (with coordination number 6) moving outside of the plane upward and downward by the same amount (0.14 Å). The resulting phonon spectrum is more symmetric than that of α'-sheet proposed by Wu *et al.*[6]. For the sake of simplicity, the buckled α-sheet will be referred to as α-sheet. The relaxed δ_6 boron sheet shows a buckling of ~0.89 Å in line with 0.82 Å obtained using the local density approximation (LDA)[10]. Boron sheets δ_5 and χ_3 are found to be flat (no buckling) in accordance with comparable studies in the literature[5,6]. For the geometry optimization process as well as the wave function calculation, a uniform k-point grid of 50×70×1, 30×30×1, 20×20×1, 30×50×1 for δ_6-, α-, δ_5-, and χ_3-boron sheets respectively were used. The dynamical matrix for the calculation of phonon frequencies are computed on a uniform q-point mesh of 7×10×1, 8×8×1, 5×5×1, 5×5×1 for δ_6-, α-, δ_5-, and χ_3-boron sheets respectively.

B. Heat capacity and ballistic thermal conductance

The phonon or electronic heat capacity at constant volume per unit area,

$$C_{phn/el}(T) = \frac{1}{A(\vec{a},\vec{b})}\left(\frac{\partial E_{phn/el}(T)}{\partial T}\right)_V$$, can be obtained from the phonon,

$$E_{phn}(T) = \sum_{\vec{q},s}\left[n_{BE}\left(\omega_s(\vec{q}),T\right)+\frac{1}{2}\right]\hbar\omega_s(\vec{q})$$, or electronic, $$E_{el}(T) = 2\sum_{\vec{k},n}n_{FD}\left(\varepsilon_n(\vec{k}),T\right)\varepsilon_n(\vec{k})$$, energy

where $\vec{q}$ is the phonon wave vector, s is the phonon mode index, $\vec{k}$ is the electron wave vector, n is

electron band index, $$n_{BE}\left(\omega_s(\vec{q}),T\right) = \left(e^{\frac{\hbar\omega_s(\vec{q})}{k_B T}}-1\right)^{-1}$$ is the Bose-Einstein distribution,

$$n_{FD}\left(\varepsilon_n(\vec{k}),T\right) = \left(e^{\frac{\varepsilon_n(\vec{k})-\varepsilon_F}{k_B T}}+1\right)^{-1}$$ is the Fermi-Dirac distribution, and $A(\vec{a},\vec{b}) = N_{\vec{q}/\vec{k}}\left\|\vec{a}\times\vec{b}\right\|$ is the sample

area, $N_{\vec{q}/\vec{k}}$ being the number of phonon or electron wave vectors in the *Brillouin* zone. This number is chosen as the number of points in the k-point sampling for the geometry optimization (see **Sec. II. A**). It

also represents the total number of unit cells. The area of a single unit cell is $\left\| \vec{a} \times \vec{b} \right\|$ where $\vec{a}$ and $\vec{b}$ are the vectors whose magnitudes are the lattice constants (see **Sec. II. A**). Ballistic thermal transport equations[14,15] sum up the individual contributions of the two heat carriers involved in the chosen thermal processes, namely, phonons (see **Eq. (1)**), and electrons (see **Eq. (2)**).

$$\kappa_{phn,\vec{\alpha}}\left(T\right) = \frac{1}{8\pi^2} \sum_s \int dq_x \int dq_y \, \hbar\omega\left(\vec{q}\right) \left| v_{\vec{\alpha},s}\left(\vec{q}\right) \right| \frac{\partial n_{BE}}{\partial T} \, , \tag{1}$$

$$\kappa_{el,\vec{\alpha}}\left(T\right) = \frac{2}{8\pi^2} \sum_n \int dk_x \int dk_y \left(\varepsilon - \varepsilon_F\right) \left| v_{\vec{\alpha},n}\left(\vec{k}\right) \right| \frac{\partial n_{FD}}{\partial T} \, , \tag{2}$$

where the phonon, $v_{\vec{\alpha},s}\left(\vec{q}\right) = \dfrac{\partial \omega_s\left(\vec{q}\right)}{\partial q_{\vec{\alpha}}}$, and electron, $v_{\vec{\alpha},n}\left(\vec{k}\right) = \dfrac{1}{\hbar} \dfrac{\partial \varepsilon_n\left(\vec{k}\right)}{\partial k_{\vec{\alpha}}}$, velocities determine the direction, $\vec{\alpha}$, of the transport x (horizontal) or y (vertical). The phonon and electron heat capacities as well as the phonon and electron ballistic thermal conductances were calculated for graphene as well.

C. Young's modulus and Poisson's ratio

Two-dimensional (2D) elastic moduli calculated through **Eq. (3)** are obtained combining the relations of longitudinal (c_L) and transverse (c_T) speeds of sound to 2D bulk (K) and shear (G) moduli[17] with the relations of 2D bulk and shear moduli to the Young's modulus (E) and the Poisson's ratio (ν)[18].

$$\left. \begin{aligned} \nu_{\alpha/\delta_5} &= 1 - \left(\frac{c_T}{c_L}\right)^2 \\[2ex] \nu_{\delta_6/\chi_3} &= \frac{\left(\dfrac{c_L}{c_T}\right)^2 - 2}{\left(\dfrac{c_L}{c_T}\right)^2 + 2} \end{aligned} \right\} \Rightarrow E = 2\left(1+\nu\right)\sigma c_T^2. \tag{3}$$

In **Eq. (3)**, the expression for ν_{α/δ_5} is chosen because of α-, and δ$_5$- sheets' hexagonal symmetry. The expression for ν_{δ_6/χ_3} is chosen because of δ$_6$- and χ$_3$ sheets' rectangular symmetry and better

ability to reproduce similar calculations through elastic constants[9]. c_L and c_T are obtained by finding the

best fitting coefficients, c_n, for the longitudinal and transverse, $\omega_{LA/TA}\left(\left|\vec{q}\right|\right) = c_0 + c_{L/T}\left|\vec{q}\right| + \sum_{n=2}^{6} c_n \left|\vec{q}\right|^n$,

acoustic dispersion relations around Γ. The surface density, $\sigma = \dfrac{N_{at}m}{\left\|\vec{a} \times \vec{b}\right\|}$, is expressed in terms of

the unit cell area, $\left\|\vec{a} \times \vec{b}\right\|$, the number of atoms per unit cell, N_{at}, and the mass of boron atom, m.

III. RESULTS AND DISCUSSION

A. Phonon and electronic spectra

The crystal structure of, the phonon and electronic spectra for δ_6- (**FIG. 1**(a)), α- (**FIG. 1**(b)), δ_5-

(**FIG. 1**(c)), and χ_3- (**FIG. 1**(d)) are evincive of their stability (no imaginary frequencies) and

metallicity (no gap around the Fermi energy level). While δ_6- and α- sheets are buckled in a manner

described in **Sec. II** and drawn in **FIG. 1**(a) and **FIG. 1**(b) with red (up) and blue (down) circles, δ_5-

and χ_3- sheets are flat in their most stable configurations. The anisotropy of δ_6- and χ_3- sheets is

observed through the difference in the dispersion relation around Γ between [$\Gamma \rightarrow X_0$] and [$\Gamma \rightarrow X_2$]

for δ_6-sheet and between [$\Gamma \rightarrow Y_0$] and [$\Gamma \rightarrow Y_2$] for χ_3-sheet. Longitudinal (LA), transverse (TA),

and flexural (ZA) acoustic branches are zoomed into the insets in the phonon spectra of **FIG.**

2(a)-(d) to highlight the area used in the polynomial fitting (**Sec. II. C**) from which sound
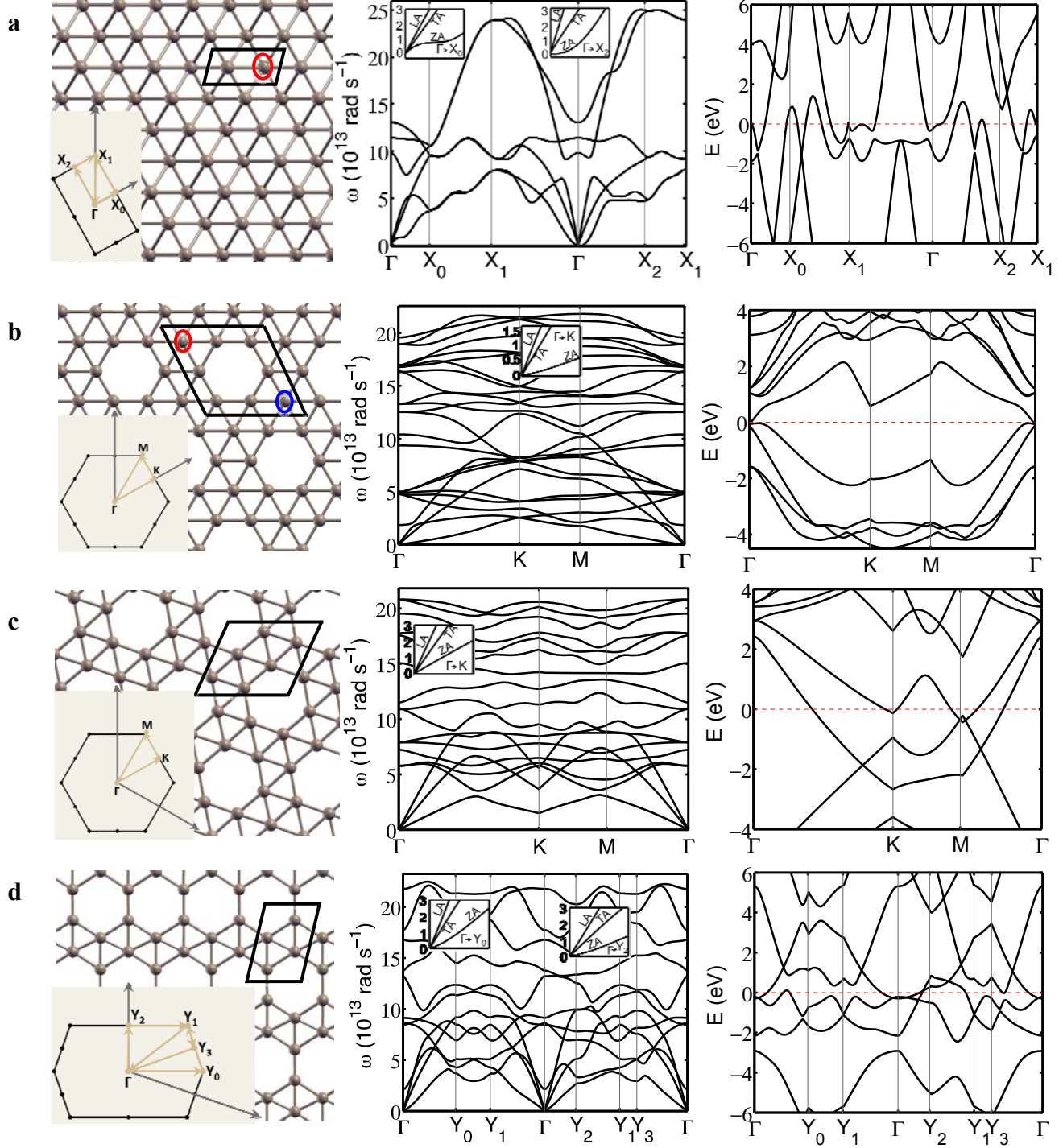
velocities are extracted.

FIG. 1. Boron sheets phonon spectra and electronic band structures. Top view and *Brillouin* zone, phonon spectrum, electronic band structure for: **(a)** δ_6 boron sheet ($\eta = 0$), **(b)** α boron sheet ($\eta = 1/9$), **(c)** δ_5 boron sheet ($\eta = 1/7$) **(d)** χ_3 boron sheet ($\eta = 1/5$). Black frames indicate the extent of the primitive cell, red circles atoms sticking out of the plane upward, blue circles atoms sticking out of the plane downward. The dashed red line is the Fermi

energy level. Acoustic branches near Γ, longitudinal (LA), transverse (TA) and flexural (ZA) are zoomed into the insets of the phonon spectra.

B. Heat capacity and ballistic thermal conductance

The detrimental effect of the vacancy density on boron sheets is observed in the phonon contribution to the heat capacity at constant volume per unit area (**FIG. 2**(a)) and the phonon contribution to the ballistic thermal conductance (**FIG. 2**(b) where both x (solid lines) and y (dashed lines) directions are considered. In fact, from δ_6 ($\eta = 0$ blue lines) and α ($\eta = 1/9$ green line) to δ_5 ($\eta = 1/7$ red line) and $\chi3$ ($\eta = 1/5$ turquoise lines), the phonon heat capacity and the phonon thermal conductance tend to decrease as the vacancy density increases.
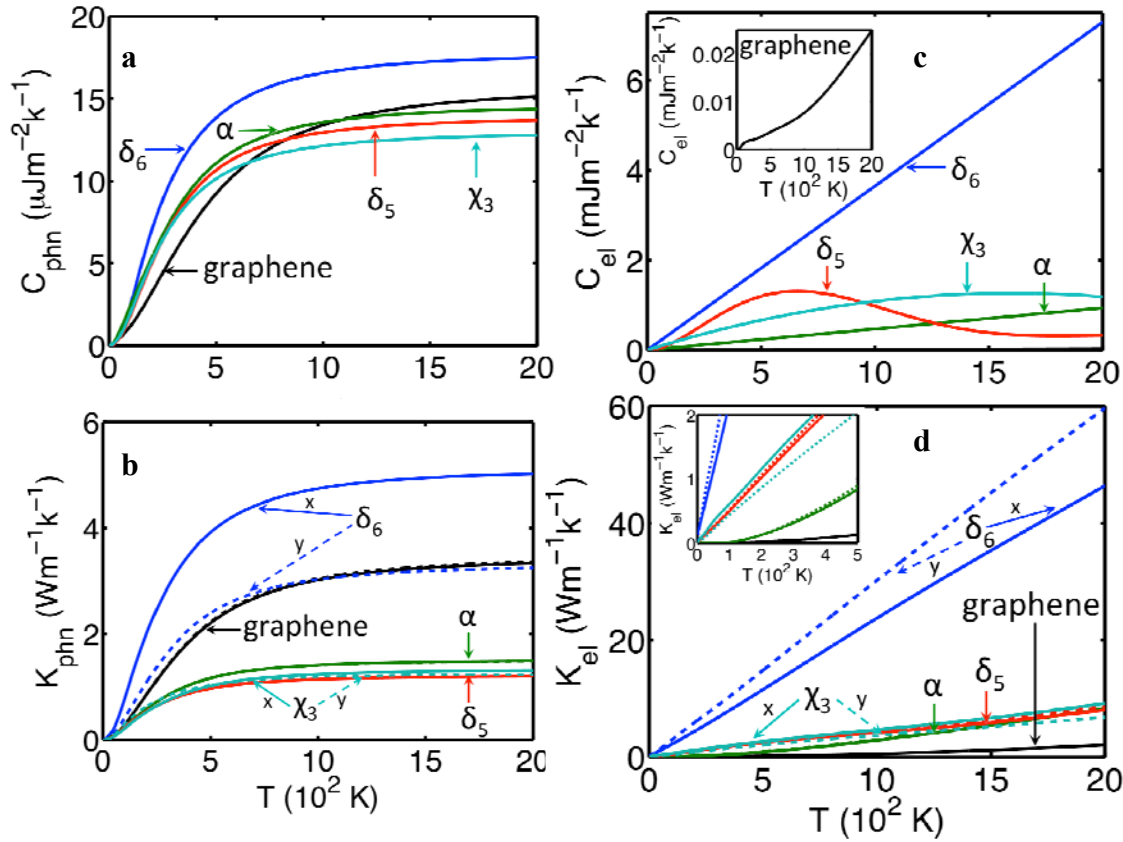

FIG. 2. **Boron sheets thermal properties.** Effect of the vacancy density, η, on the: **(a)** Phonon heat capacity at constant volume per unit area, **(b)** Ballistic phonon thermal conductance, **(c)** Electron heat capacity at constant volume per unit area, **(d)** Ballistic phonon thermal conductance. The inset in **(c)** indicates graphene's electron heat capacity per unit area roughly three orders of magnitude lower than that of boron sheets. In **(b)** and **(d)**, solid lines

refer to the x-direction and dashed lines refer to the y-direction. For graphene, α, and δ_5, solid and dashed black lines are overlapped. The inset in **(d)** further elucidates the difference of electron thermal conductance for χ_3 depending on the direction.

The calculated phonon and electron heat capacities as well as phonon and electron ballistic thermal conductances for graphene (**FIG. 2**(a)-(d)) were found to be in agreement with similar calculations in the literature[19-22]. In both phonon heat capacity at constant volume per unit area and phonon ballistic thermal conductance, while graphene is outperformed only by δ_6 (in the x-direction), an increase in the vacancy density coincides with a decrease in the lattice thermal properties. Such a behavior is related to the average interatomic distance partly responsible for the vibrational frequencies that decrease as the sheets become less dense.

Being directly proportional to the vibrational frequencies, the internal energy will decrease with the vacancy density thereby transferring the same dependence on related quantities such as the lattice heat capacity and the lattice thermal conductance, the latter being additionally contributed to by the phonon velocities. An analogical detrimental impact of the defect concentration on the thermal conductivity of silicene was revealed by a molecular dynamic study[23]. To be additionally noted is a further confirmation of the anisotropic nature of δ_6 and χ_3 as well as the isotropic nature of α and δ_5. The ratio of the x-direction phonon thermal conductance to the y-direction phonon thermal conductance in the high temperature regime (T > 1500 K) is roughly 1.55 and 1.10 for δ_6 and χ_3, respectively, and nearly 1.0 for α, δ_5 and graphene. The anisotropic behavior of δ_6 (1.55) appears to be chiefly ascribed to its profound buckling (0.89 Å) responsible for the mixing of in-plane sp^2 orbitals with out-of-plane p_z orbitals in the x-direction[4], thus favoring the phonon propagation in the said direction. The anisotropic behavior of χ_3 (1.10) can be explained in terms of the directionality of its vacancy arrangement. Looking at χ_3-sheet in the x-direction, atoms are more densely packed than they are looking at the same sheet in the y-direction, which is an indication of the heat flowing more in the former direction than in the latter direction. It is worth observing that the vacancy arrangement in both x and y directions is almost identical in α, δ_5 and graphene hence the isotropic ballistic thermal conductance observed thereof.

The regular correlation between the vacancy concentration, η, and the phonon heat capacity and thermal conductance does not occur in their electronic counterparts. Indeed, **FIG. 2**(c) and **FIG. 2**(d) does not display a regular pattern of behavior between the electronic contribution to the heat capacity or thermal conductance and the vacancy density. Unlike the case of lattice vibrations, the availability and speed of conductive electrons is independent of the vacancy density which is the reason why a regular correlation with the electron heat capacity and the electron ballistic thermal conductance has been found. It is nonetheless striking that δ_6-boron sheet have a much higher electronic heat capacity and electronic thermal conductance than all other sheets including graphene (expectedly not as metallic as boron sheets). This observation may have an explanation in terms of the morphology of the triangular sheet where because of the very small interatomic distances, in-plane sp^2 orbitals overlap much more than they do in other sheets thereby contributing to a greater orbital delocalization, itself partly responsible for both a greater number of conductive electrons and a higher electron velocity[4]. The previous considerations thus conspire to the triangular sheet's superior electron heat capacity and electron ballistic thermal conductance. It is also to be remarked that δ_6 and χ_3 preserve their anisotropic nature (see difference between solid and dashed lines) while α, δ_5, and graphene preserve their isotropic nature. This is supported by the ratio of the x-direction electron thermal conductance to the y-direction electron thermal conductance at room temperature being roughly 0.75 and 1.32 for δ_6 and χ_3, respectively, and nearly 1.0 for α, δ_5 and graphene (see **FIG. 2**(c) and **FIG. 2**(d)).

C. Young's modulus and Poisson's ratio

A correlation has been found between the vacancy density dependence of the binding energy (**TABLE II.** row 2, taken from Tang *et al.*[5]) and the calculated vacancy density dependence of the Young's modulus and speeds of sound (**TABLE II.** rows 3, 5 and 6 considering soft directions). Indeed, the Young's modulus as well as the longitudinal and transverse speeds of sound tend to relate to the vacancy density the same way the binding energy relates to the vacancy density. Besides the case of buckled triangular sheet, they all tend to decrease as the vacancy density increases. This correlation may be expected because the binding energy informs the stability and consequently the mechanical responses of the sheets.

10

A comparable study was done by Jing *et al.*[24] on graphene where an increase on the defect concentration produces a decrease in the Young's modulus, the trend of which is indicated by the binding energy.

TABLE II. Mechanical properties. Binding energies ($E_{Binding}$), Young's modulus (E), Poisson's ratio (ν), longitudinal speed of sound (c_L), and transverse speed of sound (c_T) for δ_6, α, δ_5, and χ_3.

	δ_6 ($\eta = 0$)		α ($\eta = 1/9$)	δ_5 ($\eta = 1/7$)	χ_3 ($\eta = 1/5$)	
$E_{Binding}$ (eV)	6.75[a]		6.85[a]	6.80[a]	6.58[a]	
E (N/m)	171.03[b]	194.20[c]	618.93	545.617	259.98[d]	738.26[e]
ν	1.71e-17[b]	6.05e-16[c]	0. 562	0.578	3.55e-18[d]	4.83e-18[e]
c_L (km/s)	10.52[b]	11.21[c]	17.65	16.91	15.18[d]	25.58[e]
c_T (km/s)	7.65[b]	5.54[c]	11.68	10.98	10.50[d]	15.42[e]

[a] Tang *et al.*[5]

[b] δ_6 s soft direction, [$\Gamma \rightarrow X_0$] in **FIG. 1**(a).

[b] δ_6 s hard direction, [$\Gamma \rightarrow X_2$] in **FIG. 1**(a).

[b] χ_3 s soft direction, [$\Gamma \rightarrow Y_0$] in **FIG. 1**(d).

[b] χ_3 s hard direction, [$\Gamma \rightarrow Y_2$] in **FIG. 1**(d).

The Young's moduli in **TABLE II** (second row) for δ_6- (171.03 N/m) and χ_3-sheets (256.0 N/m) in the soft directions ([$\Gamma \rightarrow X_0$] and [$\Gamma \rightarrow Y_0$] for δ_6 and χ_3 respectively) appear to be lower than those (194.20 N/m for δ_6 and 738.26 N/m for χ_3) in the hard directions ([$\Gamma \rightarrow X_2$] and [$\Gamma \rightarrow Y_2$] respectively). The aforementioned observation, although quantitatively partially in line with calculations from elastic constants[7] in the case of δ_6 (170 N/m and 398 N/m), confirms the strong anisotropy of the said sheets, from a mechanical perspective.

Longitudinal and transverse sound velocities (**TABLE II. 2** rows 5 and 6) calculated as described in **Sec. II.** and fed into **Eq. (3)** to obtain the Young's modulus and the Poisson's ratio, also follow the trend indicated by the binding energies of the sheets. In δ_6's and χ_3's hard directions, the longitudinal and transverse speeds of sound were different from those in the soft directions.

The very low Poisson's ratio for δ_6-sheet in **TABLE II.** (row 4) also appears to be in qualitative agreement with calculations from elastic constants[9]. The mechanical information about boron sheets obtained from vibrational spectra, although expectedly less quantitatively accurate than a more rigorous *ab initio* approach based on derivatives of the total energy of the layers with respect to its lattice constants, shows nonetheless an sound qualitative insight into the mechanical behavior of the sheets in relation to their intrinsic vacancy concentrations.

Overall, the correlation of the vacancy density to the mechanical and thermal properties appears directly due to the correlation between the vacancy density and the bonding arrangement discussed in physics literature[4]: the structures whose valence electrons most effectively fill in-plane sp^2 orbitals do form a stronger network of σ-bonds than the structures whose electrons partially fill weaker out-of-plane p_z orbitals[4]. Since the distribution of hexagonal holes (vacancies) and triangles determines the effectiveness of in-plane sp^2 orbital filling, it therefore further determines the stiffness/modulus of the sheet, E. The direction dependence of orbital filling on the basis of symmetry, vacancy density and buckling, originates the mechanical anisotropy observed in δ_6 and χ_3. The speed of sound is controlled by the stiffness and the mass density σ, as $c \propto \left(\dfrac{E}{\sigma}\right)^{\frac{1}{2}}$, and σ varies by only 20%, and therefore c's behavior mostly tracks the stiffness, as direct computations confirm (**TABLE II.** row 3). It is also worth noting that isotropic sheets, α and δ_5 appear to be roughly 1.7 times stiffer than graphene because the stiffness is a direct combination of the square of the transverse speed of sound and the surface density (see **Eq. (3)**). While the transverse speeds of sound (~11 km/s) for isotropic boron sheets (α and δ_5) are only 0.81 times that of graphene (13.6 km/s), their surface densities (~0.61 mg/m^2) are ~10 times that of graphene (0.063 mg/m^2) thereby leading to an expected superior stiffness. Therefore, on the basis of small variations on the transverse speed of sound, the atomic packing, related to the vacancy concentration, is an indication of the interatomic bond strength as well as the material's stiffness.

Turning once more to the thermal conductance, we note that the dense packing of the δ_6-triangular sheet logically (and per calculations) makes interatomic vibrations more rigid. This leads to higher phonons group velocities and, accordingly, greater integral transport (**Eq.** (1)), as we see indeed in **FIG.** 2(b) highest δ_6-curve. Regarding electronic contribution, again the ~3 times higher density of states in the triangular (δ_6) than in α-sheet[4], is apparently responsible for a noticeably higher electron heat capacity and electron thermal conductance seen in **FIG. 2**(c) and **FIG. 2**(d).

While noting that most of our analysis revolves around ballistic transport (which is in fact very relevant in the context of modern nanoscale devices and measurements, often in submicron range – that is likely below the mean-free path), it can be complemented by at least an estimate in the other limit of very short mean-free path. In this case, the high-temperature minimum phonon conductivity[25],

$$\kappa_{min} = \frac{1}{2}\left(\frac{\pi}{6}\right)^{\frac{1}{3}} k_B \left(\frac{N_{at}}{h\|\vec{a}\times\vec{b}\|}\right)^{\frac{2}{3}} (c_{LA} + 2c_{TA}), \; h = 3.84 \text{ Å is boron van-der-Waals diameter, provides a}$$

lower bound usually achieved in the high temperature regime. The same estimate for α and δ_5 yields greater high-T phonon conductivity (4.61 W/mK and 4.23 W/mK respectively) than for δ_6 (3.32 W/mK) and χ_3 (3.76 W/mK) in their respective soft directions, conforming to the vacancy-density dependence in **TABLE II.**

The previous ballistic-limit/small-distance analysis might encounter some discrepancies for buckled sheets (δ_6 and α) because of their puckered nature. In fact, two-dimensional out-of-plane modes (ZA) are expected to have a significant contribution to the thermal conductivity both at long and small distances as evinced in the case of graphene[26] (ZA mode contributes roughly 75% of the total thermal conductivity). However, buckled structures limit the out-of-plane vibrations insofar as the Umklapp phonon-phonon scattering time[27], $\tau_U^{ZA} \propto \exp\left(\frac{3T}{\theta_{ZA}}\right)$, is inversely proportional to the out-of-plane Debye temperature, θ_{ZA}, that tends to increase with the buckling of the structure. As a result, the more buckled the structure, the smaller the out-of-plane inelastic scattering time, τ_U^{ZA}, the more diffusive the transport and the lower the

thermal conductivity. The bucklings of stanene[28](0.86-1.1 Å), silicene[29](0.44 Å) and phosphorene[30](2.51 Å), just to name a few, are greatly responsible for a significant reduction in their thermal conductivities[31-33] in proportion to extend of the buckling. The buckling of α-boron sheet (0.14 Å) being very small compared to that of δ_6 boron sheet (0.89 Å), coupled with the binding energy difference between buckled α-boron sheet and flat α-boron sheet[6] (2 meV/atom) being very small compared to the binding energy difference between buckled δ_6-boron sheet and flat δ_6-boron sheet[10] (100 meV/atom), suggests that the aforementioned high-T ballistic limit is more likely to apply to α-boron sheet but less likely to apply to δ_6-boron sheet. Moreover, δ_6 boron sheet's superior ballistic lattice thermal conductance (roughly 2.06 times graphene lattice thermal conductance at room temperature) is likely to translate into a reduced thermal conductivity as well as a more diffusive thermal transport.

IV. SUMMARY

A study of thermal and mechanical properties of boron sheets has been presented. The study was performed feeding thermodynamic equations, ballistic Boltzmann transport formalism, and elasticity equations, the electronic and lattice spectra. Electron and phonon spectra were obtained using density functional theory (DFT) as well as density functional perturbation theory (DFPT) both implemented in the *Quantum Espresso* package[11]. A diminishing effect of the vacancy density on the heat capacity at constant volume and lattice ballistic thermal conductance is observed. A correlation between the binding energy, the Young's modulus, the Poisson's ratio, the longitudinal and transverse speeds of sound in their relationship to the vacancy density has been found. The electronic contribution to the thermal conductance was found not to have a regular relationship with the vacancy density which affects only the lattice vibrations, not the electron density.

Considering both heat carriers (phonons and electrons), the present study reveals 3 outcomes: First, phonon thermal quantities (heat capacity and thermal conductance) tend to decrease with an increase in the intrinsic vacancy concentration of boron sheets, while electron thermal counterparts appear not to have a regular correlation with it. Second, the triangular sheet's (δ_6) room-temperature phonon and electron ballistic thermal conductances (in the x-direction) are roughly 2.06 times and 6.60 times greater

14

than those of graphene, respectively. Third, α-sheet and δ_5-sheet exhibit a higher (619 N/m and 546 N/m) in-plane stiffness (2D Young's modulus) than graphene[34] (~340 N/m).

The remarkable thermal and mechanical responses of some boron sheets raise additional questions as to not-yet revealed mean free paths, scattering rates, diffusive thermal conductivity, as well as thermoelectric, magnetic, electrical, superconductive properties and their dependence on size (ribbons), morphology (sheet, cluster, tubes), chemical doping and functionalization. Answers to those questions will certainly open the door to scientific and technological breakthroughs to come.

References

1   J. Miller, Phys Today **60** (11), 20 (2007).

2   C. Ozdogan, S. Mukhopadhyay, W. Hayami, Z. B. Guvenc, R. Pandey, and I. Boustani, J Phys Chem C **114** (10), 4362 (2010).

3   E. S. Penev, S. Bhowmick, A. Sadrzadeh, and B. I. Yakobson, Nano Lett **12** (5), 2441 (2012).

4   H. Tang and S. Ismail-Beigi, Phys Rev Lett **99** (11) (2007).

5   H. Tang and S. Ismail-Beigi, Phys Rev B **82** (11) (2010).

6   X. J. Wu, J. Dai, Y. Zhao, Z. W. Zhuo, J. L. Yang, and X. C. Zeng, Acs Nano **6** (8), 7443 (2012).

7   Baojie Feng, Jin Zhang, Ro-Ya Liu, Iimori Takushi, Chao Lian, Lan Chen, Kehui Wu, Hui Li, Sheng Meng, Fumio Komori, and Iwao Matsuda,   arXiv:1512.05270 (2015).

8   Baojie Feng, Jin Zhang, Qing Zhong, Wenbin Li, Shuai Li, Hui Li, Peng Cheng, Sheng Meng, Lan Chen, and Kehui Wu, Nat Chem **advance online publication** (2016).

9   A. J. Mannix, X. F. Zhou, B. Kiraly, J. D. Wood, D. Alducin, B. D. Myers, X. L. Liu, B. L. Fisher, U. Santiago, J. R. Guest, M. J. Yacaman, A. Ponce, A. R. Oganov, M. C. Hersam, and N. P. Guisinger, Science **350** (6267), 1513 (2015).

10   J. Kunstmann and A. Quandt, Phys Rev B **74** (3) (2006).

11   P. Giannozzi, S. Baroni, N. Bonini, M. Calandra, R. Car, C. Cavazzoni, D. Ceresoli, G. L. Chiarotti, M. Cococcioni, I. Dabo, A. Dal Corso, S. de Gironcoli, S. Fabris, G. Fratesi, R.

Gebauer, U. Gerstmann, C. Gougoussis, A. Kokalj, M. Lazzeri, L. Martin-Samos, N. Marzari, F. Mauri, R. Mazzarello, S. Paolini, A. Pasquarello, L. Paulatto, C. Sbraccia, S. Scandolo, G. Sclauzero, A. P. Seitsonen, A. Smogunov, P. Umari, and R. M. Wentzcovitch, J Phys-Condens Mat **21** (39) (2009).

12   A. A. Maradudin, George H. Weiss, and E. W. Montroll, *Theory of lattice dynamics in the harmonic approximation*. (Academic Press, New York, 1963), pp.viii.

13   R. K. Pathria, *Statistical mechanics*. (Pergamon Press, Oxford, New York, 1972), pp.xiii.

14   M. H. Bae, Z. Y. Li, Z. Aksamija, P. N. Martin, F. Xiong, Z. Y. Ong, I. Knezevic, and E. Pop, Nat Commun **4** (2013).

15   E. Munoz, J. X. Lu, and B. I. Yakobson, Nano Lett **10** (5), 1652 (2010).

16   J. P. Perdew, K. Burke, and M. Ernzerhof, Phys Rev Lett **77** (18), 3865 (1996).

17   A. S. Phani, J. Woodhouse, and N. A. Fleck, J Acoust Soc Am **119** (4), 1995 (2006).

18   I. Jasiuk, J. Chen, and M. F. Thorpe, Applied Mechanics Reviews **47** (1S), S18 (1994).

19   N. Mounet and N. Marzari, Phys Rev B **71** (20) (2005).

20   K. Saito, J. Nakamura, and A. Natori, Phys Rev B **76** (11) (2007).

21   H. Mousavi and J. Khodadadi, Physica E **50**, 11 (2013).

22   K. S. Yi, D. Kim, and K. S. Park, Phys Rev B **76** (11) (2007).

23   H. P. Li and R. Q. Zhang, Epl-Europhys Lett **99** (3) (2012).

24   N. N. Jing, Q. Z. Xue, C. C. Ling, M. X. Shan, T. Zhang, X. Y. Zhou, and Z. Y. Jiao, Rsc Adv **2** (24), 9124 (2012).

25   D. G. Cahill, P. V. Braun, G. Chen, D. R. Clarke, S. H. Fan, K. E. Goodson, P. Keblinski, W. P. King, G. D. Mahan, A. Majumdar, H. J. Maris, S. R. Phillpot, E. Pop, and L. Shi, Appl Phys Rev **1** (1) (2014).

26   L. Lindsay, W. Li, J. Carrete, N. Mingo, D. A. Broido, and T. L. Reinecke, Phys Rev B **89** (15) (2014).

27   Z. Aksamija and I. Knezevic, Appl Phys Lett **98** (14) (2011).

[28] M. Modarresi, A. Kakoee, Y. Mogulkoc, and M. R. Roknabadi, Comp Mater Sci **101**, 164 (2015).

[29] Y. H. Jing, Y. Sun, H. W. Niu, and J. Shen, Phys Status Solidi B **250** (8), 1505 (2013).

[30] Q. Wei and X. H. Peng, Appl Phys Lett **104** (25) (2014).

[31] B. Peng, H. Zhang, H. Z. Shao, Y. C. Xu, X. C. Zhang, and H. Y. Zhu, Sci Rep-Uk **6** (2016).

[32] G. Z. Qin, Q. B. Yan, Z. Z. Qin, S. Y. Yue, M. Hu, and G. Su, Phys Chem Chem Phys **17** (7), 4854 (2015).

[33] X. L. Zhang, H. Xie, M. Hu, H. Bao, S. Y. Yue, G. Z. Qin, and G. Su, Phys Rev B **89** (5) (2014).

[34] C. Lee, X. D. Wei, J. W. Kysar, and J. Hone, Science **321** (5887), 385 (2008).